Low-energy effective Hamiltonian involving spin-orbit coupling in silicene and two-dimensional germanium and tin

Cheng-Cheng Liu,[1] Hua Jiang,[2,*] and Yugui Yao[1,3,†]

[1]*Institute of Physics, Chinese Academy of Sciences, Beijing 100190, China*

[2]*International Center for Quantum Materials, Peking University, Beijing 100871, China*

[3]*School of Physics, Beijing Institute of Technology, Beijing 100081, China*

(Received 15 August 2011; revised manuscript received 12 October 2011; published 7 November 2011)

Starting from symmetry considerations and the tight-binding method in combination with first-principles calculation, we systematically derive the low-energy effective Hamiltonian involving spin-orbit coupling (SOC) for silicene. This Hamiltonian is very general because it applies not only to silicene itself but also to the low-buckled counterparts of graphene for the other group-IVA elements Ge and Sn, as well as to graphene when the structure returns to the planar geometry. The effective Hamitonian is the analog to the graphene quantum spin Hall effect (QSHE) Hamiltonian. As in the graphene model, the effective SOC in low-buckled geometry opens a gap at the Dirac points and establishes the QSHE. The effective SOC actually contains the first order in the atomic intrinsic SOC strength ξ_0, while this leading-order contribution of SOC vanishes in the planar structure. Therefore, silicene, as well as the low-buckled counterparts of graphene for the other group-IVA elements Ge and Sn, has a much larger gap opened by the effective SOC at the Dirac points than graphene, due to the low-buckled geometry and larger atomic intrinsic SOC strength. Further, the more buckled is the structure, the greater is the gap. Therefore, the QSHE can be observed in low-buckled Si, Ge, and Sn systems in an experimentally accessible temperature regime. In addition, the Rashba SOC in silicene is intrinsic due to its own low-buckled geometry, which vanishes at the Dirac point K, while it has a nonzero value with deviation of $\vec{k}$ from the K point. Therefore, the QSHE in silicene is robust against the intrinsic Rashba SOC.

DOI: 10.1103/PhysRevB.84.195430 PACS number(s): 73.43.−f, 85.75.−d, 73.22.−f, 71.70.Ej

I. INTRODUCTION

Silicene, the counterpart of graphene for silicon, with slightly buckled honeycomb geometry, has been synthesized through epitaxial growth.[1] This novel two-dimensional material has attracted considerable attention both theoretically and experimentally recently, due to its exotic electronic structure and promising applications in nanoelectronics as well as its compatibility with current silicon-based electronic technology.[2–5] The structure of silicene is shown in Fig. 1. In the absence of spin-orbit coupling (SOC), the band structure of silicene shows a linear energy spectrum crossing the Fermi level around the Dirac points K and K^* of the hexagonal Brillouin zone,[2,3,5,6] which is similar to the case of graphene.

The quantum spin Hall effect (QSHE), a new quantum state of matter with nontrivial topological properties, has garnered great interest in the fields of condensed matter physics and materials science due to its scientific importance as a novel quantum state and its technological applications in spintronics.[7–9] This electronic state with time-reversal invariance is gapped in the bulk and conducts charge and spin in gapless edge states without dissipation at the sample boundaries. The existence of the QSHE was first proposed by Kane and Mele in graphene, in which SOC opens a band gap at the Dirac points.[10] Subsequent work, however, showed that the SOC is rather weak; it is in fact a second-order process of the atomic intrinsic spin-orbit interaction for graphene, and the QSHE in graphene can occur only at unrealistically low temperature.[11,12] So far, there is only one system, two-dimensional HgTe-CdTe quantum wells, where the QSHE has been demonstrated,[13,14] in spite of some other theoretical suggestions.[15,16] Recently, experimental evidence has been presented for helical edge modes in inverted InAs-GaSb quantum wells.[17,18] Nevertheless, HgTe quantum wells and other systems have more or less serious limitations such as toxicity, difficulty in processing, and incompatibility with current silicon-based electronic technology. Therefore, it is worthwhile to look for the true realization of the QSHE in silicene. Silicene and two-dimensional low-buckled honeycomb structures of germanium and tin with the QSHE are promising candidates for constructing novel spintronic devices.

Using a first-principles method, we have recently demonstrated,[5] by exploiting adiabatic continuity and the direct calculation of the Z_2 topological invariant,[19] that silicene and the two-dimensional low-buckled honeycomb structure of germanium can realize the QSHE, with a sizable gap opened at the Dirac points due to SOC and the low-buckled structure. Although the electronic structure, especially the linear energy spectrum of silicene, at low energy is similar to that of graphene,[20,21] the low-buckled geometry makes the derivation of a low-energy effective model Hamiltonian not as clear as in graphene; and the effective Hamiltonian is different from the effective Hamiltonian of surface states and thin films of a three-dimensional topological insulator.[22] Motivated by the fundamental interest associated with the QSHE and SOC in silicene, we attempt to give a low-energy effective model Hamiltonian to capture the main physics.

The paper is organized as follows. In Sec. II we briefly describe SOC in silicene from symmetry arguments. Thus, we introduce a next-nearest-neighbor tight-binding lattice model Hamiltonian to include time-reversal-invariant spin-orbit interaction. Section III presents the derivation of our low-energy effective model Hamiltonian step by step. We investigate in detail the effective spin-orbit interaction including intrinsic

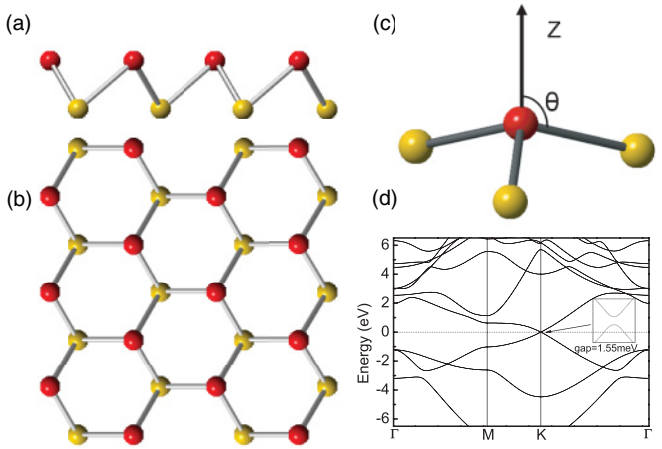

FIG. 1. (Color online) The lattice geometry of low-buckled silicene. (a),(b) The lattice geometry from the side view and top view, respectively. Note that the A sublattice (red or gray) and B sublattice (yellow or light gray) are not coplanar. (c) Definition of the angle θ as between the Si-Si bond and the z direction normal to the plane. (d) The relativistic band structure of low-buckled silicene. Inset: Zoom of the energy dispersion near the K point and the gap induced by SOC.

Rashba SOC. In Sec. IV, a comparison of the gap opened by SOC obtained from our previous first-principles results and that in the current tight-binding method is made. As an application of our model Hamiltonian, we also study the counterparts of graphene for the other group-IVA elements Ge and Sn, which are low-buckled structures according to first-principles calculations. We conclude in Sec. V with a brief discussion and summary.

II. LATTICE MODEL HAMILTONIAN INCLUDING SPIN-ORBIT COUPLING IN SILICENE FROM SYMMETRY CONSIDERATIONS

In general, SOC in the Pauli equation can be written as

$$H_{so} = \frac{\hbar}{4m_0^2c^2}(\vec{\nabla}V \times \vec{p}) \cdot \vec{\sigma} = -\frac{\hbar}{4m_0^2c^2}(\vec{F} \times \vec{p}) \cdot \vec{\sigma}, \quad (1)$$

where V ($\vec{F}$) is the potential energy (force), $\vec{p}$ is the momentum, $\hbar$ is Plank's constant, m_0 is the mass of a free electron, c is the velocity of light, and $\vec{\sigma}$ is the vector of Pauli matrices.

For graphene as shown in Fig. 2(a), the nearest-neighbor SOC is zero due to the structure's mirror symmetry with respective to an arbitrary bond, while the next-nearest-neighbor SOC is nonzero. According to symmetry,

$$H_{so} = i\gamma_2(\vec{F}_{\parallel} \times \vec{d}_{ij}) \cdot \vec{\sigma} = it_2\nu_{ij}\sigma_z, \quad (2)$$

where $\nu_{ij} = \frac{\vec{d}_i \times \vec{d}_j}{|\vec{d}_i \times \vec{d}_j|}$, γ_2 and t_2 are undetermined parameters, and $\vec{d}_i$ and $\vec{d}_j$ are the two nearest bonds connecting the next-nearest neighbors $\vec{d}_{ij}$.

For silicene, the nearest-neighbor SOC is zero, while the next-nearest-neighbor SOC is nonzero and can be divided into two parts, namely, those parallel with and perpendicular to the plane, respectively, according to the two components of the electric field force (see Fig. 2). The perpendicular component is due to the A and B sublattices being noncoplanar.

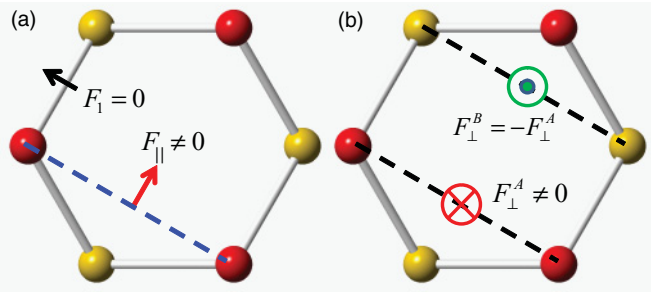

FIG. 2. (Color online) The atomic intrinsic spin-orbit interaction from symmetry considerations. (a) The nearest-neighbor force F_1 vanishes, while the next-nearest-neighbor force $\vec{F}_{\parallel}$ is nonzero in the horizontal plane. (b) The next-nearest-neighbor nonzero force $F_{\perp}^A$ equals negative $F_{\perp}^B$ in the perpendicular direction.

For the first part, the force parallel with the plane is taken into account. This case is similar to that of graphene:

$$H_{so1} = i\gamma_2(\vec{F}_{\parallel} \times \vec{d}_{ij}) \cdot \vec{\sigma} \equiv it_2\nu_{ij}\sigma_z. \quad (3)$$

For the second part, the force perpendicular to the plane is taken into account as shown in Fig. 2(b):

$$H_{so2} = i\gamma_1(\vec{\sigma} \times \vec{d}^{\,0}_{ij}) \cdot F_{\perp}^A\vec{e}_z \equiv it_1\mu_{ij}(\vec{\sigma} \times \vec{d}^{\,0}_{ij})_z, \quad (4)$$

where $\vec{d}^{\,0}_{ij} = \vec{d}_{ij}/|\vec{d}_{ij}|$, γ_1 and t_1 are undetermined parameters, and $\mu_{ij} = \pm 1$ for the A (B) site.

Finally, we introduce a second-nearest-neighbor tight-binding model:

$$H = -t\sum_{\langle ij\rangle\alpha} c^{\dagger}_{i\alpha}c_{j\alpha} + it_2\sum_{\langle\langle ij\rangle\rangle\alpha\beta} \nu_{ij}c^{\dagger}_{i\alpha}\sigma^z_{\alpha\beta}c_{j\beta} - it_1\sum_{\langle\langle ij\rangle\rangle\alpha\beta} \mu_{ij}c^{\dagger}_{i\alpha}(\vec{\sigma} \times \vec{d}^{\,0}_{ij})^z_{\alpha\beta}c_{j\beta}. \quad (5)$$

The first term is the usual nearest-neighbor hopping term. The second and third terms are the effective SOC and the intrinsic Rashba SOC. The three parameters t,t_2,t_1 are given explicit expressions in the following derivation by use of the tight-binding method.

By performing Fourier transformations, we obtain the low-energy effective Hamitoniam around the Dirac point K in the basis $\{|A\rangle,|B\rangle\} \otimes \{\uparrow, \downarrow\}$:

$$H_K^{\text{eff}} \approx \begin{pmatrix} h_{11} & v_F(k_x + ik_y) \\ v_F(k_x - ik_y) & -h_{11} \end{pmatrix}, \quad (6)$$

$$v_F = \frac{\sqrt{3}}{2}at, \quad h_{11} = -3\sqrt{3}t_2\sigma_z - \frac{3}{2}t_1a(k_y\sigma_x - k_x\sigma_y).$$

Around the Dirac point K^* in the basis $\{|A\rangle,|B\rangle\} \otimes \{\uparrow, \downarrow\}$, we have

$$H_{K^*}^{\text{eff}} \approx \begin{pmatrix} -h_{11} & v_F(k_x - ik_y) \\ v_F(k_x + ik_y) & h_{11} \end{pmatrix}. \quad (7)$$

The two effective Hamiltonians Eqs. (6) and (7) should be related by the time-reversal operation.

From the symmetry aspect analysis, we obtain the effective Hamiltonian for silicene shown as Eqs. (5)–(7). However, the magnitude of the parameters in the effective model and microscopic mechanisms such as geometry-enhanced effective SOC,[5] etc., are quite unclear. In order to study these effects, we need to construct the effective Hamiltonian from the atomic tight-binding Hamiltonian.

III. LOW-ENERGY EFFECTIVE HAMILTONIAN FROM TIGHT-BINDING THEORY

A. Low-energy effective Hamiltonian without SOC

The outer shell orbitals of silicon, namely, $3s$, $3p_x$, $3p_y$, and $3p_z$, are naturally taken into account in our analytical calculation. As shown in Fig. 1, there are two distinct sites A and B in the honeycomb lattice unit cell of silicene. Therefore, in the representation $\{|p_z^A\rangle,|p_z^B\rangle,|p_y^A\rangle,|p_x^A\rangle,|s^A\rangle,|p_y^B\rangle,|p_x^B\rangle,|s^B\rangle\}$ (for simplicity, the Dirac ket is omitted in the following) and at the K point, the total Hamiltonian in the Slater-Koster frame reads

$$H_0=\begin{pmatrix} 0 & 0 & 0 & 0 & 0 & V_3^{'} & -iV_3^{'} & 0\\ 0 & 0 & V_3^{'} & iV_3^{'} & 0 & 0 & 0 & 0\\ 0 & V_3^{'} & 0 & 0 & 0 & -V_1^{'} & -iV_1^{'} & V_2^{'}\\ 0 & -iV_3^{'} & 0 & 0 & 0 & -iV_1^{'} & V_1^{'} & -iV_2^{'}\\ 0 & 0 & 0 & 0 & \Delta & -V_2^{'} & iV_2^{'} & 0\\ V_3^{'} & 0 & -V_1^{'} & iV_1^{'} & -V_2^{'} & 0 & 0 & 0\\ iV_3^{'} & 0 & iV_1^{'} & V_1^{'} & -iV_2^{'} & 0 & 0 & 0\\ 0 & 0 & V_2^{'} & iV_2^{'} & 0 & 0 & 0 & \Delta \end{pmatrix}, \tag{8}$$

where $V_1^{'},V_2^{'},V_3^{'}$ are related to bond parameters ($V_{ss\sigma}$, etc.). The detailed derivations are shown in Appendix A. To diagonalize the total Hamiltonian, we take two steps.

First, silicene has C_3 rotational symmetry around the z axis. In order to better reflect the system's symmetry and utilize the C_3 symmetry operator, it is natural to choose spherical harmonic functions as the basis, since spherical harmonic functions are the common eigenfunctions of the Hamiltonian and the C_3 symmetry operator. Therefore, we perform the following unitary transformation:

$$\begin{aligned}
\varphi_1^A &= -\frac{1}{\sqrt{2}}\left(p_x^A+ip_y^A\right)=|p_+^A\rangle,\\
\varphi_2^B &= \frac{1}{\sqrt{2}}\left(p_x^B-ip_y^B\right)=|p_-^B\rangle,\\
\varphi_3 &= \frac{1}{\sqrt{2}}\left[-\frac{1}{\sqrt{2}}\left(p_x^A-ip_y^A\right)-\frac{1}{\sqrt{2}}\left(p_x^B+ip_y^B\right)\right],\\
\varphi_4 &= \frac{1}{\sqrt{2}}\left[\frac{1}{\sqrt{2}}\left(p_x^A-ip_y^A\right)-\frac{1}{\sqrt{2}}\left(p_x^B+ip_y^B\right)\right].
\end{aligned} \tag{9}$$

We rewrite the total Hamiltonian in the new basis $\{p_z^A,s^A,\varphi_2^B,p_z^B,s^B,\varphi_1^A,\varphi_3,\varphi_4\}$:

$$H_0 \longrightarrow H_1 = U_1^{\dagger}H_0U_1,$$

$$H_1=\begin{pmatrix} 0 & 0 & -iV_3 & 0 & 0 & 0 & 0 & 0\\ 0 & \Delta & iV_2 & 0 & 0 & 0 & 0 & 0\\ iV_3 & -iV_2 & 0 & 0 & 0 & 0 & 0 & 0\\ 0 & 0 & 0 & 0 & 0 & -iV_3 & 0 & 0\\ 0 & 0 & 0 & 0 & \Delta & -iV_2 & 0 & 0\\ 0 & 0 & 0 & iV_3 & iV_2 & 0 & 0 & 0\\ 0 & 0 & 0 & 0 & 0 & 0 & V_1 & 0\\ 0 & 0 & 0 & 0 & 0 & 0 & 0 & -V_1 \end{pmatrix}, \tag{10}$$

where U_1 is the unitary matrix that connects the new basis and the original basis, $V_1=2V_1^{'}$, $V_2=\sqrt{2}V_2^{'}$, and $V_3=\sqrt{2}V_3^{'}$.

Second, the new Hamiltonian H_1 can be separated into three decoupled diagonal blocks, which are called H_A, H_B, and H_C, respectively. H_A reads in the basis $\{p_z^A,s^A,\varphi_2^B\}$

$$H_A=\begin{pmatrix} 0 & 0 & -iV_3\\ 0 & \Delta & iV_2\\ iV_3 & -iV_2 & 0 \end{pmatrix}. \tag{11}$$

Its eigenvalues ε_1, ε_2, and ε_3 satisfy the eigenequation

$$E^3-\Delta E^2-\left(V_2^2+V_3^2\right)E+\Delta V_3^2=0. \tag{12}$$

Since this is a cubic equation, the eigenvalues and eigenvectors of H_A can be analytically obtained. We perform the unitary transformation $\{\phi_1,\phi_2,\phi_3\}\equiv\{p_z^A,s^A,\varphi_2^B\}U_A$, where

$$U_A=\begin{pmatrix} \frac{1}{\alpha_1} & \frac{1}{\alpha_2} & \frac{1}{\alpha_3}\\ \frac{V_2\varepsilon_1}{\alpha_1(\Delta-\varepsilon_1)V_3} & \frac{V_2\varepsilon_2}{\alpha_2(\Delta-\varepsilon_2)V_3} & \frac{V_2\varepsilon_3}{\alpha_3(\Delta-\varepsilon_3)V_3}\\ \frac{i\varepsilon_1}{\alpha_1V_3} & \frac{i\varepsilon_2}{\alpha_2V_3} & \frac{i\varepsilon_3}{\alpha_3V_3} \end{pmatrix}, \tag{13}$$

with the normalization factors

$$\alpha_i=\sqrt{1+\left[\frac{V_2\varepsilon_i}{(\Delta-\varepsilon_i)V_3}\right]^2+\left(\frac{\varepsilon_i}{V_3}\right)^2}.$$

For simplicity, U_A is expressed as $U_A=\{u_{ij}\}$, where u_{ij} is the matrix element of U_A. We rewrite H_A in the new basis $\{\phi_1,\phi_2,\phi_3\}$,

$$H_A\rightarrow H_A^{'}=U_A^{\dagger}H_AU_A=\begin{pmatrix} \varepsilon_1 & 0 & 0\\ 0 & \varepsilon_2 & 0\\ 0 & 0 & \varepsilon_3 \end{pmatrix}. \tag{14}$$

The above technique in H_A can also be applied to the second diagonal block H_B, which is read in the basis $\{p_z^B,s^B,\varphi_1^A\}$. H_B

satisfies the same eigenequation (12). Its eigenvalues $\varepsilon_4,\varepsilon_5,\varepsilon_6$ satisfy

$$\varepsilon_4 = \varepsilon_1, \quad \varepsilon_5 = \varepsilon_2, \quad \varepsilon_6 = \varepsilon_3. \tag{15}$$

The eigenvectors U_B of H_B are a little different from those of H_A:

$$U_B = \begin{pmatrix} u_{11} & u_{12} & u_{13} \\ -u_{21} & -u_{22} & -u_{23} \\ u_{31} & u_{32} & u_{33} \end{pmatrix}, \tag{16}$$

where u_{ij} is the matrix element in the unitary matrix U_A as presented in Eq. (13). We define the unitary transformation $\{\phi_4,\phi_5,\phi_6\} = \{p_z^B, s^B, \varphi_1^A\}U_B$. Obviously, H_B is diagonal in the new basis. H_C itself is diagonal. We define $\phi_7 \equiv \varphi_3$ and $\phi_8 \equiv \varphi_4$.

From Eq. (13) to Eq. (16), we have found a unitary transformation U_2 that connects the original basis $\{p_z^A, s^A, \varphi_2^B, p_z^B, s^B, \varphi_1^A, \varphi_3, \varphi_4\}$ and the new basis $\{\phi_1,\phi_4,\phi_2,\phi_5,\phi_3,\phi_6,\phi_7,\phi_8\}$. Under such a unitary transformation, H_1 will be diagonal.

Combining the above two steps, we finally find the new basis $\{\phi_1,\phi_4,\phi_2,\phi_5,\phi_3,\phi_6,\phi_7,\phi_8\}$ and the unitary transformation matrix $U = U_1U_2$ which diagonalize the original Hamiltonian H_0. The results are summarized as

$$\begin{aligned} &\{\phi_1,\phi_4,\phi_2,\phi_5,\phi_3,\phi_6,\phi_7,\phi_8\} \\ &\quad = \left\{p_z^A, p_z^B, p_y^A, p_x^A, s^A, p_y^B, p_x^B, s^B\right\}U, \end{aligned} \tag{17}$$

$$H_0 \rightarrow H_0' = U^\dagger H_0 U,$$

$$H_0' = \begin{pmatrix} \varepsilon_1 & 0 & 0 & 0 & 0 & 0 & 0 & 0 \\ 0 & \varepsilon_1 & 0 & 0 & 0 & 0 & 0 & 0 \\ 0 & 0 & \varepsilon_2 & 0 & 0 & 0 & 0 & 0 \\ 0 & 0 & 0 & \varepsilon_2 & 0 & 0 & 0 & 0 \\ 0 & 0 & 0 & 0 & \varepsilon_3 & 0 & 0 & 0 \\ 0 & 0 & 0 & 0 & 0 & \varepsilon_3 & 0 & 0 \\ 0 & 0 & 0 & 0 & 0 & 0 & V_1 & 0 \\ 0 & 0 & 0 & 0 & 0 & 0 & 0 & -V_1 \end{pmatrix}. \tag{18}$$

So far, the diagonal Hamiltonian has been obtained. Notice that the interesting structure is only slightly buckled, which means that V_3 is small due to the angle θ approaching 90°. When V_3 is small, the three roots of the eigenequation (12) read

$$\begin{aligned} \varepsilon_1 &\approx \Delta\frac{V_3^2}{V_2^2}, \\ \varepsilon_2 &\approx \frac{\Delta + \sqrt{\Delta^2 + 4V_2^2}}{2}, \\ \varepsilon_3 &\approx \frac{\Delta - \sqrt{\Delta^2 + 4V_2^2}}{2}. \end{aligned} \tag{19}$$

Next, we determine the Fermi energy of silicene. Due to its half filling, there are four eigenvalues below the Fermi energy. According to Eqs. (18) and (19), the eigenvalues ε_3 and V_1 are below ε_1 while the others are above ε_1, so the Fermi energy is located around ε_1. Thus, ϕ_1 and ϕ_4 are low-energy states which have the explicit forms

$$\begin{aligned} \phi_1 &= u_{11}p_z^A + u_{21}s^A + u_{31}\left[\frac{1}{\sqrt{2}}\left(p_x^B - ip_y^B\right)\right], \\ \phi_4 &= u_{11}p_z^B - u_{21}s^B + u_{31}\left[-\frac{1}{\sqrt{2}}\left(p_x^A + ip_y^A\right)\right]. \end{aligned} \tag{20}$$

In order to study the low-energy physics near the Dirac K point, we perform a small-$\vec{k}$ expansion around K via $\vec{k} \rightarrow \vec{k} + K$ and project the Hamiltonian to the representation $\{\phi_1,\phi_4\}$. We keep the first-order term in $\vec{k}$,

$$H_K = \varepsilon_1 I_2 + \begin{pmatrix} 0 & v_F k_+ \\ v_F k_- & 0 \end{pmatrix}, \tag{21}$$

with the Fermi velocity v_F,

$$\begin{aligned} v_F = \frac{-\sqrt{3}a}{2}\Big[&u_{11}^2(V_{pp\pi}\sin^2\theta + V_{pp\sigma}\cos^2\theta) - u_{21}^2 V_{ss\sigma} \\ &+ 2u_{11}u_{21}\cos\theta V_{sp\sigma} - \frac{1}{2}|u_{31}|^2\sin^2\theta(V_{pp\sigma} - V_{pp\pi})\Big], \end{aligned}$$

$$k_+ = k_x + ik_y, \quad k_- = k_x - ik_y, \tag{22}$$

where a is the lattice constant and θ is the angle between the Si-Si bond and the z direction. Notice that we have set $\hbar = 1$. So when we calculate the Fermi velocity v_F, $\hbar$ should be considered.

Equations (21) and (22) represent the final low-energy effective Hamiltonian without SOC. Two important results can obtained from these two equations. First, similar to graphene, low-buckled silicene remains gapless with linear dispersion. Second, v_F here comes originally from all the parameters $V_{pp\pi}, V_{pp\sigma}, V_{ss\sigma}, V_{sp\sigma}$, while the Fermi velocity v_F in graphene is determined only by the parameter $V_{pp\pi}$ (when $\theta = \frac{\pi}{2}$, $v_F = -\frac{\sqrt{3}}{2}V_{pp\pi}a$).

B. Low-energy effective Hamiltonian with SOC

The form of the SOC Hamiltonian H_{so} is given in the representation $\{p_z^A, p_z^B, p_y^A, p_x^A, s^A, p_y^B, p_x^B, s^B\} \otimes \{\uparrow, \downarrow\}$ (Appendix B). We know that the Hamiltonian without SOC in the basis set $\{\phi_1,\phi_4,\phi_2,\phi_5,\phi_3,\phi_6,\phi_7,\phi_8\} \otimes \{\uparrow, \downarrow\}$ is diagonal from the above depiction. The two representations are related by the unitary transformation [Eq. (17)]

$$U_{so} = U \otimes I_2, \tag{23}$$

where I_2 is the 2×2 identity matrix for the spin degree of freedom. In the representation of $\{\phi_1,\phi_4,\phi_2,\phi_5,\phi_3,\phi_6,\phi_7,\phi_8\} \otimes \{\uparrow, \downarrow\}$, the SOC Hamiltonian H_{so}' and the total Hamiltonian H' read

$$\begin{aligned} H_{so}' &\longrightarrow H_{so}' = U_{so}^\dagger H_{so} U_{so}, \\ H' &\longrightarrow H' = H_0' \otimes I_2 + H_{so}'. \end{aligned} \tag{24}$$

The first 4×4 diagonal block in the SOC Hamiltonian $H_{so}^{'}$ is no other than the first-order SOC, which reads at the Dirac point K in the basis $\{\phi_1^{\uparrow},\phi_1^{\downarrow},\phi_4^{\uparrow},\phi_4^{\downarrow}\}$

$$H_{so}^{1st} = \begin{pmatrix} -\lambda_{so}^{1st} & 0 & 0 & 0 \\ 0 & \lambda_{so}^{1st} & 0 & 0 \\ 0 & 0 & \lambda_{so}^{1st} & 0 \\ 0 & 0 & 0 & -\lambda_{so}^{1st} \end{pmatrix}, \tag{25}$$

$$\lambda_{so}^{1st} \equiv \frac{\xi_0}{2}|u_{31}|^2, \tag{26}$$

where u_{31} is the corresponding matrix element in U_A. In the following, we explain the microscopic mechanism leading to the above equation. The intrinsic effective first-order SOC can be summarized as

$$\begin{aligned} |p_{z\uparrow}^A\rangle &\xrightarrow{V} |p_{-\uparrow}^B\rangle \xrightarrow{-\frac{\xi_0}{2}} |p_{-\uparrow}^B\rangle \xrightarrow{V} |p_{z\uparrow}^A\rangle, \\ |p_{z\downarrow}^A\rangle &\xrightarrow{V} |p_{-\downarrow}^B\rangle \xrightarrow{\frac{\xi_0}{2}} |p_{-\downarrow}^B\rangle \xrightarrow{V} |p_{z\downarrow}^A\rangle, \\ |p_{z\uparrow}^B\rangle &\xrightarrow{V} |p_{+\uparrow}^A\rangle \xrightarrow{\frac{\xi_0}{2}} |p_{+\uparrow}^A\rangle \xrightarrow{V} |p_{z\uparrow}^B\rangle, \\ |p_{z\downarrow}^B\rangle &\xrightarrow{V} |p_{+\downarrow}^A\rangle \xrightarrow{-\frac{\xi_0}{2}} |p_{+\downarrow}^A\rangle \xrightarrow{V} |p_{z\downarrow}^B\rangle, \end{aligned} \tag{27}$$

where V means the nearest-neighbor direct hopping and ξ_0 represents the atomic intrinsic spin-orbit interaction strength. The whole process can be divided into three steps. Take p_z^A for example. First, due to the low-buckled structure, p_z^A couples to p_-^B [see Eqs. (11) and (20)]. The carrier in the p_z^A orbit directly hops to the nearest-neighbor p_-^B orbit. Second, when the atomic intrinsic SOC is introduced, the energy of p_-^B splits, with the spin-up carrier shifting by $-\frac{\xi_0}{2}$ while the spin-down carrier shifts by $\frac{\xi_0}{2}$. Third, the carrier in p_-^B directly hops to another nearest-neighbor p_z^A orbit. The SOC process in p_z^B is analogous to that of p_z^A except that the p_z^B orbit couples to the p_+^A orbit. The difference leads to the opposite magnitude of the effective SOC. During the whole SOC process, the atomic intrinsic SOC takes effect only once. Therefore, the effective SOC is proportional to ξ_0. A brief sketch of the process is shown in Fig. 3(b). We mainly focus on the low-buckled geometry with small V_3. According to Eqs. (13), (19), and (26), λ_{so}^{1st} reads

$$\begin{aligned} \lambda_{so}^{1st} &= \frac{\xi_0}{2}\frac{\varepsilon_1^2}{\alpha_1^2 V_3^2} \approx \frac{\xi_0}{2}\frac{2}{9}\frac{\Delta^2(V_{pp\pi}-V_{pp\sigma})^2}{V_{sp\sigma}^4} \\ &\times \frac{\cot^2\theta}{1+\frac{\cos^2\theta(V_{pp\pi}-V_{pp\sigma})^2}{V_{sp\sigma}^2}\left(1+\frac{2}{9}\frac{\Delta^2}{\sin^2\theta V_{sp\sigma}^2}\right)}. \end{aligned} \tag{28}$$

In particular, when the low-buckled geometry returns to a planar structure such as graphene ($\theta = 90^\circ$), the above formula becomes $\lambda_{so}^{1st} = 0$ and the first-order SOC vanishes. Physically, when $\theta = 90^\circ$, the p_z^A orbit is orthogonal to the p_x^B and p_y^B orbits. Therefore, the direct hopping from p_z^A to p_-^B is completely forbidden. The SOC process described in Eq. (27) cannot happen.

We also deduced the effective second-order spin-orbit interaction, whose detailed derivation is described in Appendix C. Here, we do not intend to repeat the derivation but just quote some expressions there [Eq. (C9)]:

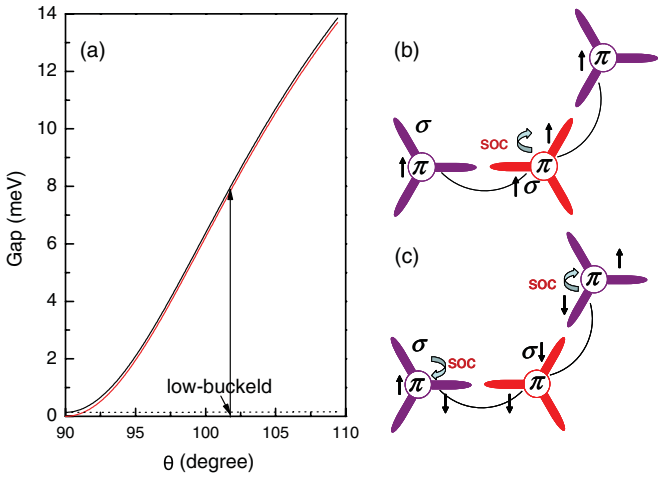

FIG. 3. (Color online) (a) The variation of the gap opened by SOC at the Dirac point with the angle θ for silicene. Black line marks the total gap. Red or gray line and dotted line mean gaps opened by the first- and second-order SOC, respectively. (b),(c) Sketches of the intrinsic effective first- and second-order spin-orbit interactions.

$$H_{so}^{2nd} = -H_n\,(H_\sigma - \varepsilon_1)^{-1}\,H_n^{\dagger}, \tag{29}$$

where H_n comprises the first to the fourth row and the fifth to the sixteenth column of $H_{so}^{'}$ above, H_σ is the direct product matrix between the lower right 6×6 diagonal matrix of $H_0^{'}$ [Eq. (18)] and the 2×2 identity matrix, and ε_1 is the eigenvalue of H_A mentioned above. When V_3 is small, the effective second-order SOC Hamiltonian reads at the Dirac point K in the basis $\{\phi_1^{\uparrow},\phi_1^{\downarrow},\phi_4^{\uparrow},\phi_4^{\downarrow}\}$

$$H_{so}^{2nd} \simeq -\lambda_{so}^{2nd} + \begin{pmatrix} -\lambda_{so}^{2nd} & 0 & 0 & 0 \\ 0 & \lambda_{so}^{2nd} & 0 & 0 \\ 0 & 0 & \lambda_{so}^{2nd} & 0 \\ 0 & 0 & 0 & -\lambda_{so}^{2nd} \end{pmatrix}, \tag{30}$$

$$\begin{aligned} \lambda_{so}^{2nd} &\equiv \left(\frac{\xi_0}{2}\right)^2 \left[\frac{|u_{11}u_{32}-u_{31}u_{12}|^2}{\varepsilon_2-\varepsilon_1} + \frac{|u_{11}u_{33}-u_{31}u_{13}|^2}{\varepsilon_3-\varepsilon_1} \right. \\ &\left. + \frac{u_{11}^2\varepsilon_1}{\varepsilon_1^2-V_1^2}\right] \\ &\approx \left(\frac{\xi_0}{2}\right)^2 \frac{2}{9}\frac{-\Delta}{\sin^2\theta V_{sp\sigma}^2}. \end{aligned} \tag{31}$$

We analyze the microscopic mechanism for λ_{so}^{2nd}. Without SOC, the low-energy H_π and the high-energy H_σ are decoupled. However, in the presence of the atomic intrinsic SOC, H_π and H_σ are coupled together. A detailed analysis shows that λ_{so}^{2nd} can be summarized as the process

$$\begin{aligned} |p_{z\uparrow}^A\rangle &\xrightarrow{\xi_0/\sqrt{2}} |p_{+\downarrow}^A\rangle \xrightarrow{V} |s_{\downarrow}^B\rangle \xrightarrow{V} |p_{+\downarrow}^A\rangle \xrightarrow{\xi_0/\sqrt{2}} |p_{z\uparrow}^A\rangle, \\ |p_{z\downarrow}^B\rangle &\xrightarrow{\xi_0/\sqrt{2}} |p_{-\uparrow}^B\rangle \xrightarrow{V} |s_{\uparrow}^A\rangle \xrightarrow{V} |p_{-\uparrow}^B\rangle \xrightarrow{\xi_0/\sqrt{2}} |p_{z\downarrow}^B\rangle, \end{aligned} \tag{32}$$

where V means the nearest-neighbor direct hopping and ξ_0 represents the atomic intrinsic spin-orbit interaction strength. During the process, the atomic intrinsic SOC takes effect twice. Thus, the effective SOC is in the second order of ξ_0. A brief sketch of the process is shown in Fig. 3(c). We note that, in graphene, the second-order $\lambda_{so}^{2\text{nd}}$ is the leading order of effective SOC and was studied in Refs. 11, 12, 21 and 23.

C. Intrinsic Rashba SOC in silicene

The extrinsic Rashba SOC in graphene is due to a perpendicular electric field or interaction with a substrate which breaks the mirror symmetry, while the intrinsic Rashba SOC in silicene is due to its own low-buckled geometry. Around the K point, the Hamiltonian containing $\vec{k}$ deviation from the K point in the representation $\{p_z^A,p_z^B,p_y^A,p_x^A,s^A,p_y^B,p_x^B,s^B\}$ reads

$$H_0(k) = \delta H_0(k) + H_0, \tag{33}$$

where H_0 is given in Eq. (8).

$$\delta H_0(k) = \begin{pmatrix} \delta h_{11} & \delta h_{12} \\ \delta h_{12}^\dagger & \delta h_{22} \end{pmatrix}, \tag{34}$$

$$\delta h_{11} = \begin{pmatrix} 0 & -v_4k_+ & 0 & 0 \\ -v_4k_- & 0 & v_3k_+ & -iv_3k_+ \\ 0 & v_3k_- & 0 & 0 \\ 0 & iv_3k_- & 0 & 0 \end{pmatrix},$$

$$\delta h_{22} = \begin{pmatrix} 0 & -v_6k_- & -iv_6k_- & v_7k_+ \\ -v_6k_+ & 0 & 0 & 0 \\ iv_6k_+ & 0 & 0 & 0 \\ v_7k_- & 0 & 0 & 0 \end{pmatrix},$$

$$\delta h_{12} = \begin{pmatrix} 0 & v_3k_- & iv_3k_- & v_5k_+ \\ -v_5k_- & 0 & 0 & 0 \\ 0 & v_2k_+ - v_1k_- & iv_1k_- & v_6k_- \\ 0 & iv_1k_- & v_2k_+ + v_1k_- & iv_6k_- \end{pmatrix},$$

$$v_1 \equiv \frac{\sqrt{3}}{8}\sin^2\theta(V_{pp\pi} - V_{pp\sigma})a,$$

$$v_2 \equiv \frac{\sqrt{3}}{4}[\sin^2\theta(V_{pp\pi} - V_{pp\sigma}) - 2V_{pp\pi}]a,$$

$$v_3 \equiv \frac{\sqrt{3}}{4}\sin\theta\cos\theta(V_{pp\pi} - V_{pp\sigma})a,$$

$$v_4 \equiv \frac{\sqrt{3}}{2}(V_{pp\pi}\sin^2\theta + V_{pp\sigma}\cos^2\theta)a,$$

$$v_5 \equiv \frac{\sqrt{3}}{2}\cos\theta V_{sp\sigma}a, \quad v_6 \equiv \frac{\sqrt{3}}{4}\sin\theta V_{sp\sigma}a,$$

$$v_7 \equiv -\frac{\sqrt{3}}{2}V_{ss\sigma}a.$$

Through the unitary transformation matrix U [Eq. (17)], in the representation $\{\phi_1,\phi_4,\phi_2,\phi_5,\phi_3,\phi_6,\phi_7,\phi_8\}$, we have

$$H_0'(k) \to H_0'(k) = U^\dagger H_0(k) U = \delta H_0'(k) + H_0', \tag{35}$$

where H_0' is given in Eq. (18). We mainly focus on the terms containing $\vec{k}$ deviation from the K point,

$$H'(k) \to H'(k) \equiv H_0'(k) \otimes I_2 + H_{so}', \tag{36}$$

where H_{so}' is given in Eq. (24). According to Eq. (C9), the total second-order Hamiltonian reads

$$H_{\text{eff}}'(k) = -H_{\text{non}}(k)(H_\sigma - \varepsilon_1)^{-1}H_{\text{non}}^\dagger(k), \tag{37}$$

where $H_{\text{non}}(k)$ comprises from the first to the fourth row and the fifth to the sixteenth column of $H'(k)$. The Hamiltonian $H_{\text{eff}}'(k)$ can be divided into two parts:

$$H_{\text{eff}}'(k) = H_{so}^{2\text{nd}} + H_R(k), \tag{38}$$

where $H_{so}^{2\text{nd}}$ is given in Eq. (30). $H_R(k)$ is the intrinsic Rashba SOC in silicene, which can be written around the Dirac point K in the basis $\{\phi_1^\uparrow,\phi_1^\downarrow,\phi_4^\uparrow,\phi_4^\downarrow\}$ as

$$H_R(k) = \begin{pmatrix} 0 & -i\lambda_R a k_- & 0 & 0 \\ i\lambda_R a k_+ & 0 & 0 & 0 \\ 0 & 0 & 0 & i\lambda_R a k_- \\ 0 & 0 & -i\lambda_R a k_+ & 0 \end{pmatrix}, \tag{39}$$

where the purely real λ_R reads

$$\begin{aligned} \lambda_R = {} & \frac{i\xi_0}{\sqrt{2}}\frac{u_{11}u_{32} - u_{31}u_{12}}{(\varepsilon_2 - \varepsilon_1)a}[(u_{12}u_{21} + u_{22}u_{11})v_5 \\ & + u_{22}u_{21}v_7 + u_{12}u_{11}v_4 - 2u_{32}u_{31}v_1] \\ & + \frac{i\xi_0}{\sqrt{2}}\frac{u_{11}u_{33} - u_{31}u_{13}}{(\varepsilon_3 - \varepsilon_1)a}[(u_{13}u_{21} + u_{23}u_{11})v_5 \\ & + u_{23}u_{21}v_7 + u_{13}u_{11}v_4 - 2u_{33}u_{31}v_1] \\ & + \xi_0\frac{u_{11}\left(u_{11}v_3 - u_{21}v_6 - \frac{i}{\sqrt{2}}u_{31}v_2\right)}{2(V_1 + \varepsilon_1)a} \\ & - \xi_0\frac{u_{11}\left(-u_{11}v_3 + u_{21}v_6 - \frac{i}{\sqrt{2}}u_{31}v_2\right)}{2(V_1 - \varepsilon_1)a}. \end{aligned} \tag{40}$$

From the above equations, we know that $H_R(k)$ is exactly zero at the Dirac point K, while $H_R(k)$ has a nonzero value when $\vec{k}$ deviates from the K point. Moreover, when the structure returns to the planar structure, $\theta = 90^\circ, \lambda_R = 0$, the intrinsic Rashba SOC vanishes even when $\vec{k}$ deviates from K. Therefore the intrinsic Rashba is entirely caused by the low-buckled geometry. The intrinsic Rashba SOC is quite different from the extrinsic Rashba SOC, which arises from a perpendicular electric field or interaction with a substrate leading to breaking of mirror symmetry in some direction, and thus has finite magnitude at the Dirac point K.

IV. RESULTS AND DISCUSSION

Finally, taking into account Eqs. (21), (25), (30), and (39), we obtain the entire low-energy effective Hamiltonian around

TABLE I. An application of the low-energy effective Hamiltonian [Eq. (41)]. The terms of this general low-energy effective Hamiltonian are given for these different systems corresponding to the different angles θ of the lowest-energy geometry. The lattice constants a and angles θ for the lowest-energy geometry are obtained from first-principles calculation. The values of λ_{so}^{1st}, λ_{so}^{2nd}, and λ_R caused by the low-buckled geometry and SOC at the Dirac point K are obtained from our tight-binding model using the hopping parameters in Table II. The gap opened by SOC at the Dirac point K is obtained from first-principles and the current tight-binding method. We also give the carrier Fermi velocity v_F around the Dirac point K from first-principles and the current tight-binding method.

System	a (Å)	θ (deg)	λ_{so}^{1st} (meV)	λ_{so}^{2nd} (meV)	λ_R (meV)	Gap (TB) (meV)	Gap (FP) (meV)	v_F (TB) (10^5 m/s)	v_F(FP)(10^5 m/s)
Graphene	2.46	90	0	1.3×10^{-3}	0	2.6×10^{-3}	0.8×10^{-3}[a]	9.80	8.46
Silicene	3.86	101.7	3.9	7.3×10^{-2}	0.7	7.9	1.55[b]	5.52	5.42
Ge(licene)	4.02	106.5	43	3.3	10.7	93	23.9[b]	4.57	5.24
Sn(licene)	4.70	107.1	29.9	34.5	9.5	129	73.5	4.85	4.70

[a]Reference 11.
[b]Reference 5.

the Dirac K point acting on the low-energy states ϕ_1 and ϕ_4:

$$H_K^{\text{eff}}(\theta) = H_K \otimes I_2 + H_{so}^{1st} + H_{so}^{2nd} + H_R(k) = \left(\varepsilon_1 - \lambda_{so}^{2nd}\right) I_4 + \begin{pmatrix} h_{11} & v_F k_+ \\ v_F k_- & -h_{11} \end{pmatrix}, \quad (41)$$

$$h_{11} \equiv -\lambda_{so}\sigma_z - a\lambda_R(k_y\sigma_x - k_x\sigma_y),$$

where I_2 is the 2×2 identity matrix for the spin degree of freedom, I_4 is the 4×4 identity matrix, $\lambda_{so} = \lambda_{so}^{1st} + \lambda_{so}^{2nd}$, and v_F is given in Eq. (22). Through the time-reversal operation, the entire low-energy effective Hamiltonian around the Dirac K^* point reads

$$H_{K^*}^{\text{eff}}(\theta) = \left(\varepsilon_1 - \lambda_{so}^{2nd}\right) I_4 + \begin{pmatrix} -h_{11} & v_F k_- \\ v_F k_+ & h_{11} \end{pmatrix}. \quad (42)$$

The effective Hamiltonian deduced from the atomic tight-binding method has asimilar formula to that derived from symmetry considerations. Comparing Eqs. (41) and (6), we obtain

$$t = \frac{2\sqrt{3}v_F}{3a}, \quad t_2 = \frac{\lambda_{so}}{3\sqrt{3}}, \quad t_1 = \frac{2}{3}\lambda_R. \quad (43)$$

The parameters t, t_2, t_1 are undetermined in the second-nearest-neighbor tight-binding model [Eqs. (5) and (6)] from the symmetry analysis. Here, from Eqs. (22), (28), (31), (40), and (43), we can not only give their explicit expressions, but also specify the magnitudes of the three parameters through v_F, λ_{so} ($\lambda_{so} = \lambda_{so}^{1st} + \lambda_{so}^{2nd}$), and λ_R, whose values are presented in Table I. In the following, we discuss the physical meaning of our low-energy effective Hamiltonian. First of all, the low-energy effective Hamiltonian is analogous to the first proposal of the QSHE in graphene except for the intrinsic Rashba SOC term $H_R(k)$.[19] The SOC-inducing mass term in the Hamiltonian opens a gap at the Dirac points. Moreover, from K to K^* the mass term changes its sign and the band is inverted. Therefore, the low-buckled silicene is also a QSHE system. The QSHE can be observed experimentally when the Fermi energy is located inside the gap and the temperature is below the minimal gap energy. The existence of the QSHE in silicene has been studied in our recent work using the first-principles method combined with a direct Z_2 calculation.[5]

Second, the energy gap in low-buckled silicene is much larger than that in graphene. Equation (41) results in a spectrum $E(\vec{k}) = \pm\sqrt{(v_F^2 + a^2\lambda_R^2)k^2 + \lambda_{so}^2}$. Therefore, the energy gap is $2\lambda_{so}$ at the Dirac points. Due to the low-buckled geometry, not only the second-order SOC λ_{so}^{2nd} but also the much larger first-order SOC λ_{so}^{1st} exists. In Fig. 3, we show the variation of the gap with the angle θ. When θ deviates from 90°, the gap induced by λ_{so}^{2nd} for silicene is nearly unchanged while the gap induced by λ_{so}^{1st} increases rapidly. The larger is the angle, the greater is the gap. In particular, the gap can reach several meV for just a little buckling, and therefore the QSHE can be observed in an experimentally attainable temperature regime. It is noted that this paper mainly focuses on the intrinsic properties of free-standing silicene while the effects of the environment, especially a substrate, are not considered. When silicene is on a substrate or in a perpendicular electric field, extrinsic Rashba SOC may appear due to the broken mirror symmetry. The Rashba SOC caused by interaction with a substrate is more complicated to estimate. However, if one assumes that the interaction is a weak van der Waals interaction, the Rashba SOC can be expected to be much smaller than intrinsic SOC. Moreover, the extrinsic Rashba SOC due to a perpendicular electric field may be written as $\lambda_R = \frac{eE_z z_0}{3V_{sp\sigma}}\xi_0$,[12] where z_0 is proportional to the atomic size of silicon. Its magnitude is about 0.2 meV if we assume a typical electric field[10] $E_z \sim (50\text{ V})/(300\text{ nm})$ and use the value $z_0 \sim 4.5a_B$. Therefore, in silicene, the magnitude of the intrinsic SOC at 1.55 meV is much larger than that of the extrinsic Rashba SOC. Through comparing the strength of the extrinsic Rashba SOC to that of the intrinsic SOC, one can verify that extrinsic Rashba SOC will not affect the survival of the QSHE.

Third, due to the low-buckled geometry, the effective Hamiltonian also contains the intrinsic Rashba SOC term. This term leads to interesting properties. On the one hand, since it vanishes at the Dirac point, the minimal bulk energy gap $2\lambda_{so}$ will not be affected by the intrinsic Rashba SOC. Therefore, it does not diminish the temperature window for experimental observation of the QSHE in silicene. On the other hand, due to the nonzero values of the Rashba SOC term, spin is not a good quantum number. Thus, the spin Hall conductance is no longer quantized in silicene. The intrinsic Rashba SOC is entirely different from the extrinsic Rashba SOC, which has

TABLE II. The magnitudes of hopping parameters. The energy units are eV. The strength of SOC ξ_0 is obtained from first-principles calculation except for Sn.

System	$V_{ss\sigma}$	$V_{sp\sigma}$	$V_{pp\sigma}$	$V_{pp\pi}$	Δ	ξ_0
Graphene	− 6.769	5.580	5.037	− 3.033	− 8.868[a]	9×10^{-3}[c]
Silicene	− 1.93	2.54	4.47	− 1.12	− 7.03[b]	34×10^{-3}[d]
Ge(licene)	− 1.79	2.36	4.15	− 1.04	− 8.02[b]	0.196
Sn(licene)	− 2.6245	2.6504	1.4926	− 0.7877	− 6.2335[e]	0.8[f]

[a]Reference 25.
[b]Reference 26.
[c]Reference 11.
[d]Reference 5.
[e]Reference 27.
[f]Reference 28.

a finite value at the Dirac point K. The presence of intrinsic Rashba SOC may provide a way to manipulate the spin in silicene without destroying its QSHE state.

Fourth, the entire low-energy effective Hamiltonian applies not only to the silicene itself but also to the low-buckled counterparts of graphene for the other group-IVA elements Ge and Sn, as well as to graphene with planar geometry. These different structures correspond to different angles θ. Therefore, in this sense, the effective Hamiltonian is quite general.

The values in Table I of $\lambda_{so}^{1st}, \lambda_{so}^{2nd}, \lambda_R$, the gap, and v_F caused by SOC at the Dirac point K in graphene, silicene, gelicene, and snlicene (corresponding to two-dimensional low-buckled Ge and Sn) are obtained from the tight-binding method by using the typical parameter values from Table II. Notice that λ_{so}^{2nd} is slightly larger than λ_{so}^{1st} in snlicene due to the huge SOC strength with the magnitude of eV, while λ_{so}^{2nd} is much smaller than λ_{so}^{1st} in the other systems. For comparison, we present the corresponding gaps from the first-principles method too, which agree with our tight-binding method results in order of magnitude. We also give the carrier Fermi velocity v_F around the Dirac point K from first principles and from the current tight-binding method. Since we only focus on the low-buckled geometry, our calculation shows that the carrier Fermi velocity does not significantly change with θ.

Notice that those bond parameters presented in Table II and used in Table I come from the corresponding diamond structure (sp^3 hybridization) except for the graphene (sp^2) case. However, considering that low-bulk structures are closer to sp^2 hybridization and the bond parameters of sp^2 hybridization will be a little different from those of sp^3 hybridization, through slight improvement of these bond parameters we expect that the tight-binding gap would better match the first-principles results.

V. SUMMARY

In summary, based on symmetry aspects and the tight-binding method combined with first-principles calculation, we derived the low-energy effective Hamiltonian for silicene, which is very general because this Hamiltonian applies not only to silicene itself but also to the low-buckled counterparts of graphene for the other group-IVA element Ge and Sn, as well as to graphene where the structure returns to the planar geometry. The low-energy effective Hamiltonian does indeed exhibit the QSHE, with a form similar to that of Kane and Mele's first graphene QSHE Hamiltonian except for the intrinsic Rashba SOC term $H_R(k)$. However, the effective SOC in low-buckled geometry is actually first order in the atomic intrinsic SOC strength ξ_0, while the planar structure in graphene leads to the vanishing of the leading-order contribution. Therefore, silicene and the low-buckled counterparts of graphene for the other group-IVA elements Ge and Sn have much larger gaps opened by the effective SOC at the Dirac point than graphene due to the low-buckled geometry and larger atomic intrinsic SOC strength. Further, the larger is the angle, the greater is the gap. Therefore, the QSHE can be observed in an experimentally accessible low-temperature regime in these low-buckled systems. In addition, the Rashba SOC in silicene is intrinsic due to its own low-buckled geometry, which vanishes at the Dirac point K, while it has a nonzero value when $\vec{k}$ deviates from the K point. As a result, although the spin Hall conductance is not quantized, the QSHE in silicene is robust against such intrinsic Rashba SOC. This is entirely different from the extrinsic Rashba SOC due to a perpendicular electric field or interaction with a substrate, which is independent of $\vec{k}$, has finite value at the Dirac points, and is detrimental to the QSHE.

ACKNOWLEDGMENTS

We would like to thank Qian Niu, Junren Shi, and Haiwen Liu for helpful discussions. This work was supported by NSF of China (Grant No. 10974231), the MOST Project of China (Grants No. 2007CB925000 and No. 2011CBA00100), CPSF Grant No. 20100480147, and the 985 Program of Peking University.

APPENDIX A: H_0 MATRIX

In the representation $\{p_z^A, p_z^B, p_y^A, p_x^A, s^A, p_y^B, p_x^B, s^B\}$ the total Hamiltonian reads

$$H_0 = \begin{pmatrix} \mathbf{H}_\pi & \mathbf{H}_n \\ \mathbf{H}_n^\dagger & \mathbf{H}_\sigma \end{pmatrix}, \qquad \mathbf{H}_\sigma = \begin{pmatrix} \mathbf{E} & \mathbf{T} \\ \mathbf{T}^\dagger & \mathbf{E} \end{pmatrix}. \tag{A1}$$

Here, $\mathbf{H}_\pi$ and $\mathbf{H}_\sigma$ are 2×2 and 6×6 matrices, respectively. The nondiagonal block $\mathbf{H}_n$ coupling $\mathbf{H}_\pi$ and $\mathbf{H}_\sigma$ is a 2×6 matrix. In the following derivation, the energy level of the $3p$ orbital is set as the energy zero point. The matrix $\mathbf{E}$ describing the on-site energy of different atomic orbitals can be written as

$$\mathbf{E}=\begin{pmatrix}0&0&0\\0&0&0\\0&0&\Delta\end{pmatrix}, \tag{A2}$$

where Δ is the energy difference between the $3s$ and $3p$ orbitals. Actually, for the sake of simplicity, here we have assumed that these bases are orthogonal when centered on different sites. We choose the coordinate system in which the unit cell has primitive vectors

$$\vec{a}_1=a\left(\frac{1}{2},\frac{\sqrt{3}}{2}\right),\quad \vec{a}_2=a\left(-\frac{1}{2},\frac{\sqrt{3}}{2}\right). \tag{A3}$$

The lattice constant a is defined as the nearest distance between lattice points in the same sublattice, which is 3.86 Å for silicene from our first-principles calculation.[5] The three nearest-neighbor translation vectors are

$$\begin{aligned}\vec{d}_1&=\frac{a}{\sqrt{3}}\left(\frac{\sqrt{3}}{2},\frac{1}{2},\cot\theta\right),\\ \vec{d}_2&=\frac{a}{\sqrt{3}}\left(-\frac{\sqrt{3}}{2},\frac{1}{2},\cot\theta\right),\\ \vec{d}_3&=\frac{a}{\sqrt{3}}(0,-1,\cot\theta).\end{aligned} \tag{A4}$$

As shown in Fig. 1, the angle θ is defined as being between the Si-Si bond and the z direction normal to the plane. The corresponding reciprocal lattice vectors are

$$\vec{b}_1=\frac{2\pi}{a}\left(1,\frac{\sqrt{3}}{3}\right),\quad \vec{b}_2=\frac{2\pi}{a}\left(-1,\frac{\sqrt{3}}{3}\right). \tag{A5}$$

The Dirac point K is chosen to be $\vec{K}=\frac{1}{3}(\vec{b}_1-\vec{b}_2)=(\frac{4\pi}{3a},0)$, and $K^*=-K$. The matrix $\mathbf{T}$ describes the hopping between two sublattices, which is given in Table III by the Slater-Koster formula.[24] In Table III, the four bond parameters $V_{ss\sigma}$, $V_{sp\sigma}$, $V_{pp\sigma}$, and $V_{pp\pi}$ correspond to the σ and π bonds formed by $3s$ and $3p$ orbitals, whose numerical values given in Table II specify our model quantitatively. The hopping matrix elements in the momentum space read

$$t(k)=\sum_{i=1}^{3}t(\vec{d}_i)e^{i\vec{k}\cdot\vec{d}_i}. \tag{A6}$$

TABLE III. The matrix elements for the nearest-neighbor hopping between s and p orbitals are considered as functions of the direction cosine l, m, and n of the vector from the left orbital to the right orbital. Other matrix elements are found by permuting indices.

$t_{s,s}$	$V_{ss\sigma}$	$t_{x,x}$	$l^2V_{pp\sigma}+(l-l^2)V_{pp\pi}$
$t_{s,x}$	$lV_{sp\sigma}$	$t_{x,y}$	$lm(V_{pp\sigma}-V_{pp\pi})$
$t_{x,s}$	$-lV_{sp\sigma}$	$t_{y,z}$	$mn(V_{pp\sigma}-V_{pp\pi})$

Therefore, the matrices $\mathbf{T}$ and $\mathbf{H}_n$ at the Dirac point K can be written as

$$\mathbf{T}=\begin{pmatrix}-V_1^{'}&-iV_1^{'}&V_2^{'}\\-iV_1^{'}&V_1^{'}&-iV_2^{'}\\-V_2^{'}&iV_2^{'}&0\end{pmatrix}, \tag{A7}$$

$$\mathbf{H}_n=\begin{pmatrix}0&0&0&V_3^{'}&-iV_3^{'}&0\\V_3^{'}&iV_3^{'}&0&0&0&0\end{pmatrix}, \tag{A8}$$

$$\begin{aligned}V_1^{'}&\equiv\frac{3}{4}\sin^2\theta(V_{pp\pi}-V_{pp\sigma}),\\ V_2^{'}&\equiv\frac{3}{2}\sin\theta V_{sp\sigma},\\ V_3^{'}&\equiv\frac{3}{2}\sin\theta\cos\theta(V_{pp\pi}-V_{pp\sigma}).\end{aligned}$$

The matrix $\mathbf{H}_\pi$ at the Dirac point K reads

$$\mathbf{H}_\pi=\begin{pmatrix}0&0\\0&0\end{pmatrix}. \tag{A9}$$

Consequently, the Hamiltonian H_0 is obtained.

APPENDIX B: H_{so} MATRIX

When in center field, Eq. (1) reads

$$H_{so}=\xi_0\vec{L}\cdot\vec{s}. \tag{B1}$$

The above equation can also be written as

$$H_{so}=\xi_0\left(\frac{L_+s_-+L_-s_+}{2}+L_zs_z\right), \tag{B2}$$

where $s_\pm=s_x\pm is_y$ denote the positive (negative) operator for spin and $L_\pm=L_x\pm iL_y$ denote the positive (negative) operator for the angular momentum in the selected basis. The SOC on the same atom is taken into account. The concrete SOC term can be obtained by calculating the mean value of Eq. (B2). For example, the SOC term between $|p_z\uparrow\rangle$ and $|p_x\downarrow\rangle$ reads $\langle p_z\uparrow|H_{so}|p_x\downarrow\rangle=-\frac{\xi_0}{2}$, etc.[29] During the derivation we may take advantage of the following expressions:

$$\begin{aligned}L_+|l,m\rangle&=[l(l+1)-m(m+1)]^{1/2}|l,m+1\rangle,\\ L_-|l,m\rangle&=[l(l+1)-m(m-1)]^{1/2}|l,m-1\rangle,\\ L_z|l,m\rangle&=m|l,m\rangle,\end{aligned} \tag{B3}$$

where l and m represent the azimuthal and magnetic quantum numbers, respectively. A straightforward calculation leads to the on-site SOC in the representation $\{p_z^A,p_z^B,p_y^A,p_x^A,s^A,p_y^B,p_x^B,s^B\}\otimes\{\uparrow,\downarrow\}$:

$$H_{so}=\frac{\xi_0}{2}\times h_{so}. \tag{B4}$$

All elements in h_{so} can be found in Table IV.

APPENDIX C: THE SECOND-ORDER EFFECTIVE HAMILTONIAN

In general, the Hamiltonian reads

$$\mathbb{H}=\begin{pmatrix}H_\pi&H_n\\H_n^\dagger&H_\sigma\end{pmatrix}. \tag{C1}$$

TABLE IV. The values of SOC among atomic orbitals that are used in h_{so}. A,B denote the two distinct sites. The nonzero SOC terms only exist at the same site. $\sigma_{x,y,z}$ are Pauli matrices acting on the spin space. O denotes the zero matrix.

	$p_z^{A/B}$	$p_y^{A/B}$	$p_x^{A/B}$	$s^{A/B}$
$p_z^{A/B}$	O	$i\sigma_x$	$-i\sigma_y$	O
$p_y^{A/B}$	$-i\sigma_x$	O	$i\sigma_z$	O
$p_x^{A/B}$	$i\sigma_y$	$-i\sigma_z$	O	O
$s^{A/B}$	O	O	O	O

We focus on the following case: (i) the eigenvalues of H_π are around energy ϵ while the eigenvalues of H_σ are far away from ϵ; (ii) the energy scale of the nondiagonal block H_n is much smaller than the eigenvalue value difference between H_π and H_σ. The effective Hamiltonian around energy ϵ (or the second-order effective Hamiltonian for H_π) can be obtained by the following method.[30] $\mathbb{H}$ can be rewritten as

$$\mathbb{H} \equiv \epsilon I + \mathbb{H}_0 + \mathbb{H}_{\text{non}}, \tag{C2}$$

$$\mathbb{H}_0 = \begin{pmatrix} H_\pi - \epsilon & 0 \\ 0 & H_\sigma - \epsilon \end{pmatrix}, \quad \mathbb{H}_{\text{non}} = \begin{pmatrix} 0 & H_n \\ H_n^\dagger & 0 \end{pmatrix}.$$

For simplicity, we omit the unitary matrix I in the above and in the following derivation. In order to obtain the effective Hamiltonian, one may perform a canonical transformation:

$$\mathbb{H} \to H_S = e^{-S}\mathbb{H}e^S,$$

$$S = \begin{pmatrix} 0 & M \\ -M^\dagger & 0 \end{pmatrix}, \tag{C3}$$

where the matrix M is determined by

$$[\mathbb{H}_0, S] + \mathbb{H}_{\text{non}} = 0. \tag{C4}$$

Through a simple algebraic derivation, we have

$$(H_\pi - \epsilon)M - M(H_\sigma - \epsilon) + H_n = 0. \tag{C5}$$

Therefore, we can find a recursive expression for M,

$$\begin{aligned} M &= [H_n + (H_\pi - \epsilon)M](H_\sigma - \epsilon)^{-1} \\ &= H_n(H_\sigma - \epsilon)^{-1} + (H_\pi - \epsilon)H_n(H_\sigma - \epsilon)^{-2} + \cdots . \end{aligned} \tag{C6}$$

We know that in silicene the eigenvalues of $H_\sigma - \epsilon$ determined by the energy of H_σ separated from those of H_π are of order eV near the K point, while the energy scale of $H_\pi - \epsilon$ is nearly zero and H_n is of order meV for SOC. Therefore the above recursive expression can be written as

$$M \approx H_n(H_\sigma - \epsilon)^{-1}. \tag{C7}$$

The transformed Hamiltonian has the following approximate form:

$$\begin{aligned} H_S = e^{-S}\mathbb{H}e^S &= \mathbb{H} + [\mathbb{H}, S] + \tfrac{1}{2!}[[\mathbb{H}, S], S] + \cdots \\ &= \epsilon I + \mathbb{H}_0 + \tfrac{1}{2}[\mathbb{H}_{\text{non}}, S] + \cdots . \end{aligned} \tag{C8}$$

Up to the second order, the final effective Hamiltonian for H_π can be written as

$$\begin{aligned} H_{\text{eff}} &\simeq H_\pi - \tfrac{1}{2}(H_n M^\dagger + M H_n^\dagger) \\ &\simeq H_\pi - H_n(H_\sigma - \epsilon)^{-1} H_n^\dagger. \end{aligned} \tag{C9}$$

*jianghuaphy@gmail.com
†ygyao@aphy.iphy.ac.cn

[1] B. Lalmi, H. Oughaddou, H. Enriquez, A. Kara, S. Vizzini, B. Ealet, and B. Aufray, Appl. Phys. Lett. **97**, 223109 (2010).
[2] P. De Padova, C. Quaresima, C. Ottaviani, P. M. Sheverdyaeva, P. Moras, C. Carbone, D. Topwal, B. Olivieri, A. Kara, H. Oughaddou *et al.*, Appl. Phys. Lett. **96**, 261905 (2010).
[3] S. Cahangirov, M. Topsakal, E. Aktürk, H. Sahin, and S. Ciraci, Phys. Rev. Lett. **102**, 236804 (2009).
[4] Y. Ding and J. Ni, Appl. Phys. Lett. **95**, 083115 (2009).
[5] C. C. Liu, W. Feng, and Y. Yao, Phys. Rev. Lett. **107**, 076802 (2011).
[6] G. G. Guzmán-Verri and L. C. Lew Yan Voon, Phys. Rev. B **76**, 075131 (2007).
[7] M. Z. Hasan and C. L. Kane, Rev. Mod. Phys. **82**, 3045 (2010).
[8] X. Qi and S. Zhang, Phys. Today **63**(1), 33 (2010).
[9] X. Qi and S. Zhang, Rev. Mod. Phys. **83**, 1057 (2011).
[10] C. L. Kane and E. J. Mele, Phys. Rev. Lett. **95**, 226801 (2005).
[11] Y. Yao, F. Ye, X. L. Qi, S. C. Zhang, and Z. Fang, Phys. Rev. B **75**, 041401 (2007).
[12] H. Min, J. E. Hill, N. A. Sinitsyn, B. R. Sahu, L. Kleinman, and A. H. MacDonald, Phys. Rev. B **74**, 165310 (2006).
[13] B. A. Bernevig, T. L. Hughes, and S. Zhang, Science **314**, 1757 (2006).
[14] M. König, S. Wiedmann, C. Brüne, A. Roth, H. Buhmann, L. W. Molenkamp, X. Qi, and S. Zhang, Science **318**, 766 (2007).
[15] S. Murakami, Phys. Rev. Lett. **97**, 236805 (2006).
[16] C. Weeks, J. Hu, J. Alicea, M. Franz, and R. Wu, Phys. Rev. X **1**, 021001 (2011).
[17] C. Liu, T. L. Hughes, X. L. Qi, K. Wang, and S. C. Zhang, Phys. Rev. Lett. **100**, 236601 (2008).
[18] I. Knez, R. Du, and G. Sullivan, Phys. Rev. Lett. **107**, 136603 (2011).
[19] C. L. Kane and E. J. Mele, Phys. Rev. Lett. **95**, 146802 (2005).
[20] A. K. Geim and K. S. Novoselov, Nat. Mater. **6**, 183 (2007).
[21] A. H. Castro Neto, F. Guinea, N. M. R. Peres, K. S. Novoselov, and A. K. Geim, Rev. Mod. Phys. **81**, 109 (2009).
[22] W. Shan, H. Lu, and S. Shen, New J. Phys. **12**, 043048 (2010).
[23] D. Huertas-Hernando, F. Guinea, and A. Brataas, Phys. Rev. B **74**, 155426 (2006).
[24] J. C. Slater and G. F. Koster, Phys. Rev. **94**, 1498 (1954).
[25] R. Saito, M. Fujita, G. Dresselhaus, and M. S. Dresselhaus, Phys. Rev. B **46**, 1804 (1992).

[26]W. A. Harrison, *Electronic Structure and the Properties of Solids: The Physics of the Chemical Bond* (Dover, New York, 1989).

[27]T. G. Pedersen, C. Fisker, and R. V. Jensen, J. Phys. Chem. Solids **71**, 18 (2010).

[28]D. J. Chadi, Phys. Rev. B **16**, 790 (1977).

[29]C. X. Liu, X. L. Qi, H. J. Zhang, X. Dai, Z. Fang, and S. C. Zhang, Phys. Rev. B **82**, 045122 (2010).

[30]R. Winkler, *Spin-Orbit Coupling Effects in Two-Dimensional Electron and Hole Systems*, 1st ed. (Springer, Berlin, 2003).